OVERVIEW OF ROTARY FLOW VISUALIZATION RESULTS ON THE F/A-18 AIRCRAFT

H. J. Cai and M. E. Beyers
Aerodynamics Laboratory, Institute for Aerospace Research,
National Research Council Canada

Keywords: *vortex flow field, high angles of attack, rotary testing, F/A-18*

Abstract

To understand the physics of the complex vortex flow field of the F/A-18 aircraft during maneuvering at high incidences, a series of flow visualizations were conducted in the IAR 0.38 x 0.51m water tunnel. A 1/72-scale model was tested on the new orbital-platform rotary apparatus at angles of attack from 20° to 65° with sideslip angles in the range ± 10°. It was found that the aerodynamic behaviour of the F/A-18 aircraft is dominated by forebody/LEX vortex interactions. Strong or weak leeward vortex interactions occur at different rotation rates and sideslip angles, causing non-linear lateral-directional aerodynamic behaviour. The boundaries of the threshold rotation rates at post-stall angles of attack and non-zero sideslip have been defined by the flow visualization results. Asymmetric forebody vortex shedding occurred at 57.5° ≤ α ≤ 65° under static conditions. The rotary vortex flow field exhibits hysteretic behaviour over the range of steady rotation rates.

1 Introduction

The flow field about the F/A-18 aircraft flying at high angles of attack is typically dominated by extensive three-dimensional flow separation. Many experimental and analytical investigations have contributed to the understanding of the aerodynamics in this flow regime [1-10]. Because of the cross-coupling of the forebody and LEX vortices the flow field is characterized by multiple interacting vortices. Considerable benefit can be derived from the presence of these vortices and their interactions. Current fighter aircraft actually exploit vortex flows for enhanced maneuverability at high angles of attack [8,10]. However, the interaction of multiple vortices increases the complexity of the global flow field, particularly in sideslip or in coning motion [11] and introduces new problems. Much attention has been focused on the severe tail buffet environment of the F/A-18 at 15° < α < 30º, which is generated from the interaction of the vortical flows with the vertical stabilizers [10].

In addition, the F/A-18 has experienced control problems during maneuvering at angles of attack in the range 40°< α < 50º and higher [12]. Current simulator models have difficulty in predicting departure from controlled flight, indicating that there is considerable potential for enhancing simulator fidelity [9,12]. Moreover, the F/A-18 aircraft is susceptible to wing rock at angles of attack around 40º to 45º [6]. Thus, to understand the mutual interactions of the vortices is essential for successful prediction of the behaviour of the aircraft at high angles of attack.

Flow visualization in water tunnels provides an excellent means for detailed observation of the flow around a wide variety of configurations. Whereas in many instances this introduces scaling problems, the F/A-18 is something of an exception. In Ref. 12 it is shown that F/A-18 post-stall aerodynamic results obtained at laminar water tunnel conditions are representative of full-scale flight at Mach numbers from 0.2 to 0.4 and angles of attack α in the range 30° ≤ α ≤ 50°. Favorable correlations of water tunnel and full-scale data

obtained are due to the unique forebody/LEX geometry of the F/A-18. These findings corroborate results from previous investigations [5,7,8], which had revealed that the flight test results at high angles of attack agreed quite well with the ground test results at low Reynolds numbers (Re). Consequently, water tunnels have become highly useful facilities for critical evaluation of complex flow fields on this aircraft.

Following comprehensive force tests [11,14,15], a series of flow visualization experiments on a 1/72-scale F/A-18 model were undertaken in the IAR 0.38 x 0.51 m water tunnel [11,13,15,16]. Emphasis was placed on understanding the forebody/LEX vortex interactions, and defining the effect of the rotation rate and sideslip angle β on the lateral-directional aerodynamic behaviour, and in particular, on the rolling moment characteristics.

2 Experimental Equipment

The experiments were conducted in the IAR 0.38 x 0.51m water tunnel (Fig. 1).

A 1/72-scale plastic kit model of the F/A-18 used for flow visualization tests (Fig. 2) was fitted with 12 dye ports. The test model was in the baseline fighter-escort configuration and incorporated a 34° leading-edge flap deflection. The model featured flow-through engine inlets and a distorted aft fuselage assembly to allow the installation of a sting.

An advanced orbital platform apparatus (OPLEC) [11,13] was used for rotary experiments. The model was mounted on a sting attached to an annular "orbital platform" riding on the outer surface of a stationary cylindrical test section insert. This configuration results in minimal aerodynamic interference by virtue of the absence of the rotating support arm, or C-strut, found in conventional rotary rigs. Two indexing spacers were used to set the bank angle ϕ at discrete values in intervals of 2.5° in the range $-50° \leq \phi \leq 50°$ [14]. The relationship between the angles α, β and σ, ϕ is

$$\alpha = \tan^{-1}(\tan\sigma \cos\phi) \quad (1)$$

$$\beta = \sin^{-1}(\sin\sigma \sin\phi) \quad (2)$$

where σ is the pitch angle.

Two CCD cameras provided side and bottom views of the test section. Each camera has its own dedicated PC for streaming the video data to hard disk. The motion control card in the data acquisition PC simultaneously triggered the cameras.

3 Results and Discussing

3.1 Basic Static Flow Field Characteristics

3.1.1 LEX vortex breakdown location

The LEX vortex breakdown location is sensitive to the pressure gradient and, therefore, a function of angle of attack. As α is increased, the LEX vortex breakdown longitudinal location x/l moves forward while the lateral location moves slightly inboard (Fig. 3)(l is the model length and the longitudinal coordinate x is measured aft of the nose).

At α = 15° LEX vortex breakdown occurs at the wing trailing edge (Fig. 3a). Turbulence downstream of the breakdown point envelops the entire surface of the vertical stabilizers. At α = 28° the breakdown point has moved close to the LEX / wing junction (Fig. 3b). The rapid movement of the breakdown point between α = 28° and α = 30° (Fig. 3c) suggests that a critical point lies within this range. At higher angles of attack (Fig. 3d) breakdown approaches the LEX apex, and reaches it at α ≅ 50°. However, at this condition the breakdown positions are no longer symmetrical owing to "vortex cross-interaction", discussed in section 3.2.

The static measurements of LEX vortex breakdown location were correlated with wind tunnel, water tunnel and flight data [5,15]. The results from the NASA Dryden HARV flight tests and IAR water tunnel tests are in good agreement (Fig. 4). A data fit of x/l as function

of α for the F/A-18 aircraft at β = 0 yields for 15° ≤ α ≤ 50°

$$x/l = 1.31 - 0.0396\,\alpha + 0.000379\,\alpha^2$$

where α is in degrees.

3.1.2 Angle-of-attack effect on forebody vortices

The forebody vortex system of F/A-18 is clearly visible at α ≥ 25° (Fig 5a). With increasing angle of attack, the forebody vortex core is displaced further from the model surface, while the vortex breakdown location moves forward, from near the leading edge of the vertical stabilizers at α = 30° (Fig. 3c) to just aft of the canopy at α = 50° (Fig. 5c). There was some hint of asymmetric vortex shedding at α = 55°. The asymmetric vortices were fully developed at α = 57.5° (Fig. 5d). Vortex flow was observed on the forebody up to α = 65° (Fig. 5f), and at α ≥ 70° wake-like flow was observed (Fig. 5g).

3.1.3 Interaction between LEX and forebody vortices

The strong interactions between the forebody and wing/LEX vortex systems can dominate the F/A-18 aerodynamic characteristics [17]. The present tests show that at 30° ≤ α < 45° the forebody vortex is pulled down beneath the stronger LEX vortex and deflected outboard (Fig. 3 and 5). As the angle of attack increases, the interaction location moves forward. At α ≥ 45° the forebody vortex crossed over intermittently to the opposite side to interact with the spiral LEX flow (after breakdown) on that side (Fig. 3f).

The location of the vortex interaction is defined as the point along the longitudinal axis where the forebody vortex core first exhibits a sharp change in its curvature, as viewed from either the side or the top of the model. Figure 6 shows the favourable correlation of the forebody/LEX vortex interaction locations obtained from water tunnel and flight tests.

3.2 Rotary Flow Field Characteristics

Coning motion creates a velocity distribution that produces local sideslip and upwash flow around the model. This results in stronger LEX-induced upwash on the windward (advancing) side (in the lateral sense), and weaker upwash on the leeward (retreating) side [18]. As a result, the windward forebody vortex tends to lift off the surface during coning motion. At constant α the windward LEX vortex breakdown location was found to travel forward and inboard, while the leeside breakdown location travelled aft and outboard.

In the range 30° ≤ α < 45°, the vortex systems remain symmetric at low non-dimensional rotation rates, $\Omega = \dot{\Phi}\, b/2U_\infty$, where $\dot{\Phi}$ is the coning rate and b is the wingspan. At Ω = 0.05 the leeside body vortex becomes entrained into the leeside LEX vortex, whereas the windward body vortex is sheared away from the fuselage. The interaction occurring between the leeside body vortex and the swirling flow of the leeward burst LEX vortex is referred to as a "weak" interaction [15] (Fig.7b, 8b). As the rotation rate increased to a certain value the interaction occurred before breakdown, which is termed a "strong" interaction (Figs. 7c, 8c and 9c). The mean longitudinal LEX vortex breakdown locations on the windward and leeward sides at α = 30° are shown in Fig. 10. At Ω = 0.2, the difference between the two sides is $\Delta(x/l) \cong 0.1$. The various vortex interactions between the forebody and wing/LEX vortex systems dominate the aerodynamic characteristics, resulting in non-linear lateral-directional aerodynamic behaviour. At the low Ω, corresponding to weak interaction, the rolling moments are not significantly affected. At high enough Ω, the rolling moments increase significantly with increasing Ω [11,14].

In the α range from 45° to 50°, the LEX vortex lateral positions are generally close on the two sides of the rotating model, except at intermediate values of Ω (0.025 < |Ω| < 0.15). In this α and Ω range the attached vortex on the leeward side crosses over toward the windward side under the influence of the sidewash

generated by the lifted vortex (Fig. 9a,b). This is termed "vortex cross-interaction" [15]. As a result of the presence of the attached forebody vortex the upwash on the windward side is apparently reduced, causing a delay of LEX vortex breakdown. Figure 10 shows the breakdown locations on windward side at $\alpha = 45^\circ$ moving forward at $\Omega > 0.1$. The vortex cross-over occurred consistently in the range of $0.1 \leq |\Omega| \leq 0.15$ at $\alpha = 45^\circ$, extending to $|\Omega| \leq 0.2$ at $\alpha = 52.5^\circ$. It is evident that this would result in a redistribution of the lateral aerodynamic loading.

Careful analysis of a large number of video flow visualization records yielded the data characterizing the vortex interactions over the $\alpha - \Omega$ range, as summarized in Fig. 11 [16]. At low Ω and $\alpha \leq 42.5°$ essentially symmetric forebody vortex shedding occurs. A "neutral-unsteady" condition occurs at $\alpha \geq 45°$. Beyond the range $-0.05 \leq \Omega \leq 0$ the coning rate dominates and the forebody vortex on the advancing side detaches from the surface. At substantial rotation rates in the range $45° \leq \alpha \leq 55°$ the attached vortex crosses over to interact with the LEX vortex on the advancing side. As Ω is increased the interaction switches to the same side. In general, the strong interactions occur at rotation rates $|\Omega| \geq 0.15$. There is a tendency for the minimum rate for strong interactions to increase with increasing α. The regions of symmetric, direct- and cross-vortex interaction are separated by regions of unsteadiness. "Unsteady vortex crossover" refers to the regions in which intermittent cross-vortex interaction occurs, while "unsteady vortex asymmetry" refers to conditions at $\alpha \geq 52.5^\circ$, where the forebody vortex asymmetry can no longer lead to interactions with the LEX vortices.

3.3 Flow Field Hysteresis Effects at High Angles of Attack

At angles of attack for asymmetric vortex shedding $\alpha > \alpha_{AV}$ ($\cong$ 55°), the test results showed that the flow field depends significantly on α and Ω. At low rotation rates, the effects of flow field inertia are dominant. A variety of different types of behaviour was observed at $|\Omega| \leq 0.2$. For the example at $\alpha = 60°$, an asymmetric vortex pair had formed at $\Omega = 0$ and its orientation had been set by a combination of forebody micro-asymmetry and tunnel flow angularity, with the starboard forebody vortex lifted. At low rotation rates, the asymmetric vortex system remained in its original orientation, even after the rotation direction had changed (Figs.12a,b). This behaviour disappeared when Ω was increased to 0.225, at which point the vortex asymmetry switched immediately when the rotation direction was reversed (Fig. 12c,d). This change in flow state is associated with the existence of a threshold rotation rate Ω_T [19]. The different types of behaviour observed at $|\Omega| < \Omega_T$ may be summarized as follows:

(1) locked-in forebody vortex asymmetry (no bifurcation) (Fig. 12f).
(2) intermittent switching between the two bistable positions, causing bifurcation in the lateral-directional loads (Fig. 12h).
(3) unsteady conditions near $|\Omega| = \Omega_T$ with no evident asymmetric vortex shedding (Fig. 12g)

These results, together with the differences in Reynolds number, can explain the different types of lateral-directional aerodynamic characteristics at $\alpha = 60°$, observed in the IAR [14] and NASA facilities [2,3]. The yawing moment (C_n) characteristics appear in Fig. 13.

3.4 Sideslip Effects on the Vortical Interactions

The sideslip angle introduces changes in effective leading-edge sweep angle on the two sides. This results in the windward LEX vortex breakdown moving forward, inboard and closer to the LEX surface, while the leeward vortex breakdown moves aft, outboard and higher above the LEX surface. The leeside primary separation line shifts down and on the windward side it shifts up. Moreover, the leeside forebody vortex travels aft beside the canopy and then curves down to merge with the

LEX vortex. The windward forebody vortex passes closer to the top of the forebody and canopy and, at high sideslip angles, crosses over the body centre line to the other side.

As sideslip angle increased, the leeside forebody vortex interacts with the LEX vortex further forward, while on the windward side it is further aft. In addition, the leeside forebody vortex is located lower along the side of the canopy and closer to the LEX vortex. Thus, it is more susceptible to interaction with the LEX vortex, compared with the windward side [5]. Various patterns of vortical interactions between the LEX vortices and forebody vortices were observed at sideslip. Figure 14 shows the interaction modes at $\sigma = 35°$ and three bank angles, $\phi = 0$, -10° and -17.5°. The vortex interaction locations at $\beta \neq 0$ and $30° < \alpha < 35°$ measured in water tunnel and flight tests [5] are in good agreement (Fig. 15).

In rotary motion, the overall velocity distribution results from the combination of body-axes sideslip and local coning-induced sideslip effects. With different combinations of positive or negative Ω and ϕ, the sideslip effect on forebody/LEX vortex interaction might be augmented or cancelled out. The boundaries of steady-state flow interactions in the range of σ from 30° to 52.5° and $\beta = \pm 10°$ were derived from flow visualization observations [16]. As an example, Fig. 16 shows the $\sigma = 40°$ case, illustrating the aerodynamic behaviour for the aircraft at post-stall angles of attack. The rolling moment (C_ℓ) behaviour is most interesting, showing nonlinear and anti-symmetric trends over the σ range $35° \leq \sigma \leq 45°$, in particular. The C_ℓ characteristics at $\sigma = 40°$ are shown in Fig. 17, together with the associated flow visualization results. At $\phi = 0$ ($\beta = 0$) C_ℓ has an inflection point at $\Omega = 0$, corresponding to the "symmetric" vortex systems shown in Fig. 17(a). At $\Omega \geq 0.1$, C_ℓ increases with increasing Ω, as a result of the leeward strong vortex interaction due to coning motion (as Fig. 17(b) shows at $\Omega = 0.2$). However, when $\phi > 0$, for instance $\phi = 15°$ ($\alpha \cong 40°$, $\beta \cong 10°$), the inflection point is shifted to $\Omega < 0$ (Fig. 17(d)), where the two vortex systems are again "symmetric" at $\Omega = -0.1$. When a vortex cross-interaction occurred at $\Omega = -0.2$ (Fig. 17(c)), a positive increment in C_ℓ results. At $\Omega \geq -0.025$, strong vortex interactions occur (Figs. 17(e) and (f)).

4 Conclusions

The use of an advanced OPLEC apparatus for flow visualization in a water tunnel provided the opportunity for further understanding the flow physics of the F/A-18 in coning motion in the post-stall regime. The test results have revealed new details of the F/A-18 rotary flow field characteristics, which were not previously available. The following conclusions may be drawn.

(1) At $30° < \alpha < 50°$, strong interactions between forebody and LEX vortices are generated on the leeward (retreating) side at rotation rates above a threshold value $|\Omega| \geq \Omega_T$. The threshold rotation rate is a function of angle of attack and sideslip.
(2) In the range $45° \leq \alpha \leq 55°$ and at low Ω, the leeward forebody vortex frequently crosses over to the opposite side at zero sideslip. This results in a change in sign of the lateral-directional loads.
(3) For $57.5° \leq \alpha \leq 65°$, the flow around the model is dominated by asymmetric forebody vortex shedding. Above the threshold, Ω_T, the windward forebody vortex is invariably lifted off the surface, but below the threshold, $|\Omega| < \Omega_T$, three different types of unsteady behaviour are observed.
(4) The effect of sideslip and coning rate on the flow field are coupled, and consistent with a trend to shift the lateral-directional characteristics to different Ω values.
(5) Boundaries for the occurrence of the various steady-state vortical flow interactions could be determined.

Acknowledgement

This project was funded in part by Defence R&D Canada. The authors wish to recognize

the contribution of Capt. Doug Baker, DTA 3-4-3, scientific authority for the project.

References

[1] Erickson, G. E., Water Tunnel Flow Visualization and Wind Tunnel Data Analysis of the F/A-18, *NASA CR-165859*, 1982.

[2] Hulzburg, R., Low Speed Rotary Aerodynamics of F-18 Configuration for 0 to 90 Angle of Attack-Test Results and Analysis, *NASA CR 3608*, Aug. 1984.

[3] Kramer, B. R., Suarez, C. J., Malcolm, G.N. and Ayers, B. F., F/A-18 Forebody Vortex Control, Volume 2- Rotary-Balance Tests, *NASA CR 4582*, March 1994.

[4] Murman, S. M., Schiff, L. B. and Rizk, Y. M., Numerical Simulation of the Flow about an F-18 Aircraft in the High-Alpha Regime, *AIAA Paper 93-3405*, Aug. 1993.

[5] Del Frate, J. H. and Zuniga, F. A., In-Flight Flow Field Analysis on the NASA F-18 High Alpha Research Vehicle with Comparisons to Ground Facility Data, *AIAA Paper 90-0231*, Jan.1990.

[6] Fisher, D. F., Del Frate, J. H. and Richwine D. M., In-Flight Flow Visualization Characteristics of the NASA F-18 High Alpha Research Vehicle at High Angles of Attack, *NASA TM 4193*, May 1990.

[7] Sandlin, Dr. Doral R. and Ramirez, Edgar J., A Water Tunnel Flow Visualization Study of the Vortex Flow Structures on the F/A-18 Aircraft, *NASA-CR-186938*, July 1991.

[8] David F.Fisher, John H.Del Frate and Fanny A. Zuniga, Summary of In-flight Flow Visualization Obtained from the NASA High Alpha Research Vehicle (HARV), *NASA TM 101734*.

[9] Beyers, M.E., F/A-18 Nonplanar Maneuvering Aerodynamics, *46th Annual Conference of CASI*, Montreal, May 1999, pp. 95-107.

[10] Erickson, G. E., Del Frate, J. H., Hanley, R.J. and Pulley, C. T. etc., Experimental Investigation of the F/A-18 Vortex Flows at Subsonic Through Transonic Speeds (invited Paper), *AIAA 89-2222* CP, 1989.

[11] Cai, H. J. and Beyers, M. E., OPLEC Rotary Experiments on the F/A-18, *NRC, IAR-LTR-A-021*, March 1998.

[12] Beyers, M.E., From Water Tunnel to Post-Stall Flight Simulation-the F/A-18 Investigation, accepted for publication in *Journal of Aircraft*, 2002.

[13] Cai, H. J., Beyers, M. E. and O'Hagan, S., An Orbital Platform Rotary Balance System for IAR Water Tunnel, *ICIASF '97 Record*, Sept. 1997, pp.236-245.

[14] Cai, H. J., Beyers, M. E., OPLEC Investigation of F/A-18 High-Alpha Aerodynamic Nonlinearities, *NRC IAR LTR-A-046*, March 2000.

[15] Beyers, M. E., Cai, H. J.,F/A-18 Post-Stall Aerodynamic Database, *NRC IAR LTR-AL-0088*, December 2001.

[16]. Cai, H. J., Beyers, M. E., OPLEC Rotary Flow Visualization Study of F/A-18 at Zero Sideslip, *NRC IAR LTR-A-042*, August 1999.

[17] Erickson, G. E. and Gilbert, W. P., Experimental Investigation of Forebody and Wing Leading-Edge Vortex Interactions at High Angles of Attack, *AGARD CP 342*, July 1983.

[18] Ericsson, L. E. and Beyers, M. E., Wind Tunnel Aerodynamics in Rotary Tests of Combat Aircraft Models, *Journal of Aircraft*, Vol.35, No. 4, 1998, pp. 521-528.

[19] Beyers, M. E. and Ericsson, L. E., Extraction of Subscale Free-Flight Aerodynamics from Rotary Tests of Combat Aircraft, *AIAA 97-0730*, Jan. 1997.

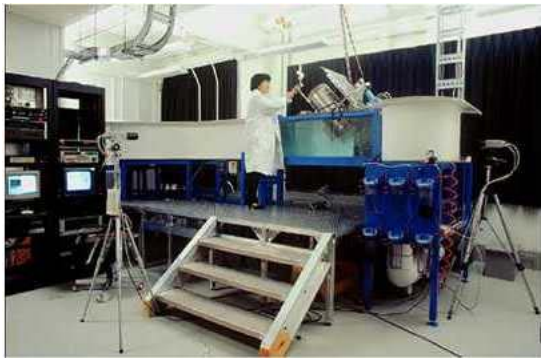

Fig.1 General arrangement of experimental equipment in IAR water tunnel

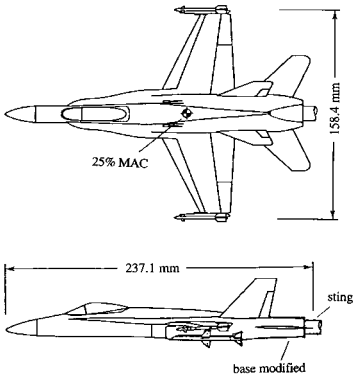

Fig. 2 1/72 scale F/A-18 model

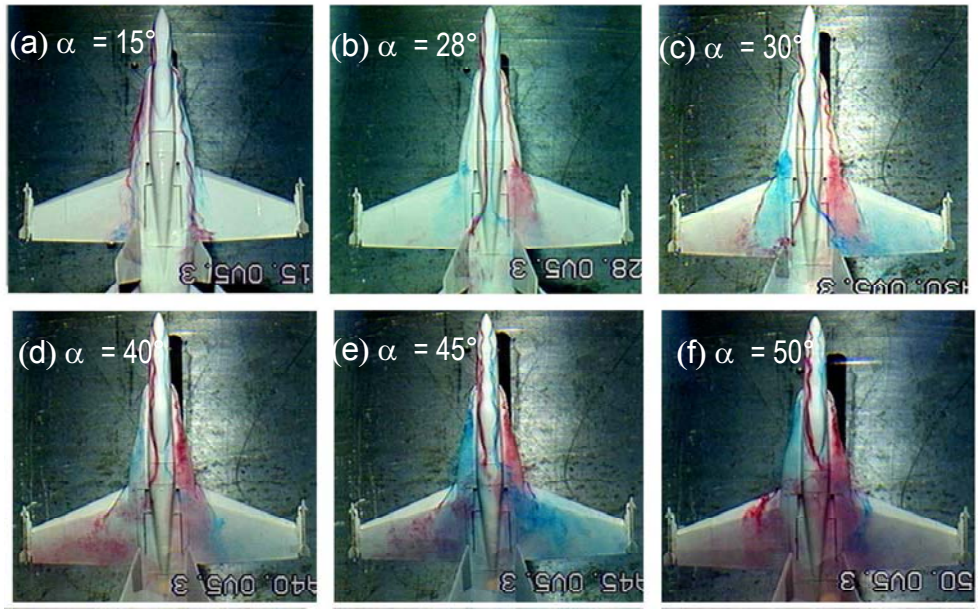

Fig. 3 Static flow pattern (top view)

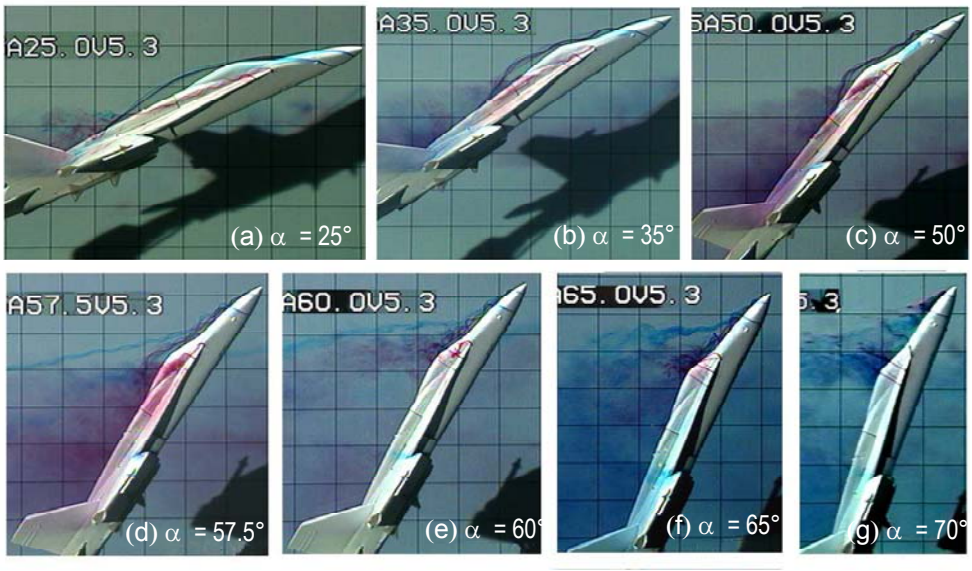

Fig. 5 Static flow pattern (side view)

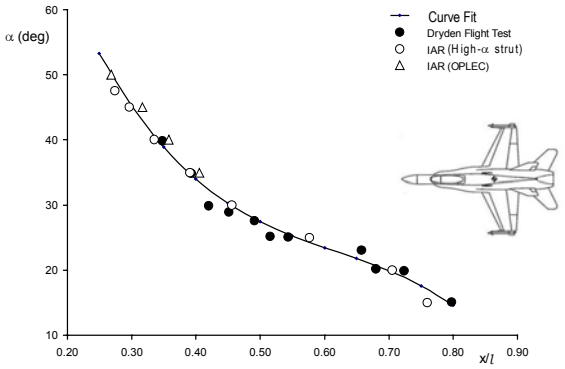

Fig. 4 Correlation of F/A-18 vortex breakdown position in IAR water tunnel and in flight

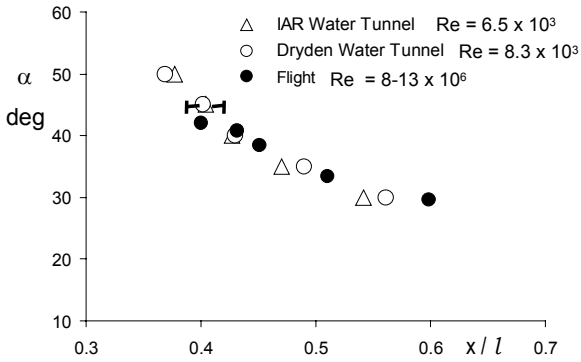

Fig. 6 Comparison between vortex interaction point in water tunnel and flight (β = 0)

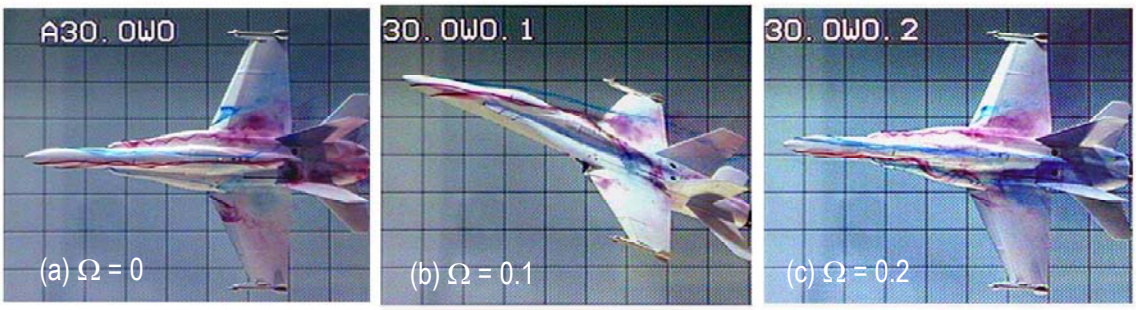

Fig. 7 Rotary flow pattern at $\alpha = 30°$

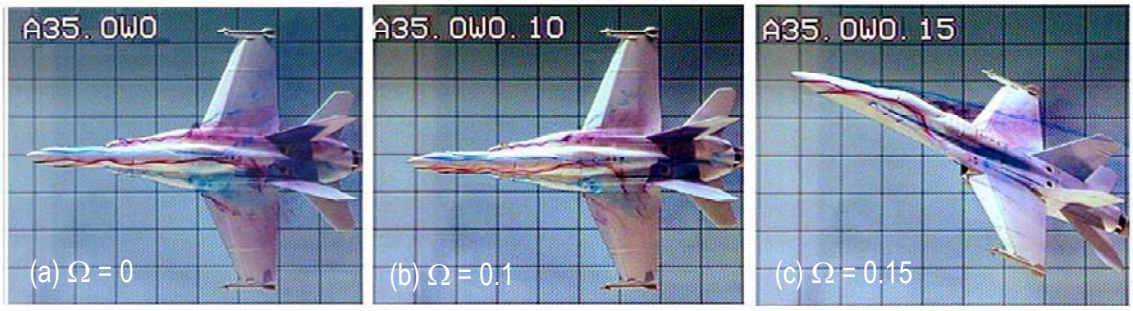

Fig. 8 Rotary flow pattern at $\alpha = 35°$

Fig. 9 Rotary flow pattern at $\alpha = 45°$

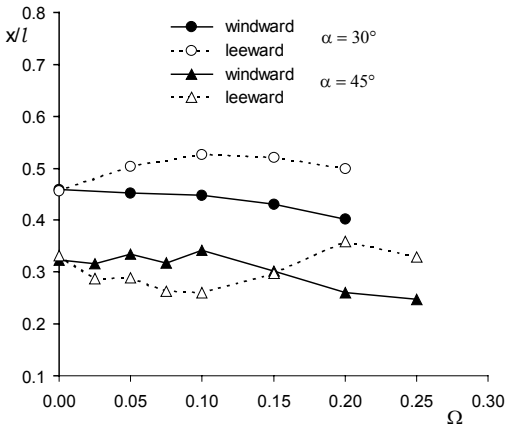

Fig. 10 Effect of rotation on the LEX vortex breakdown locations at $\alpha = 30°$ and 45°

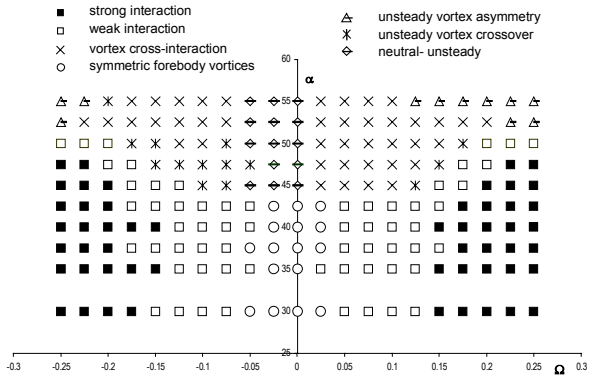

Fig. 11 Map of forebody / LEX vortex interaction conditions for coning model at $\beta = 0$

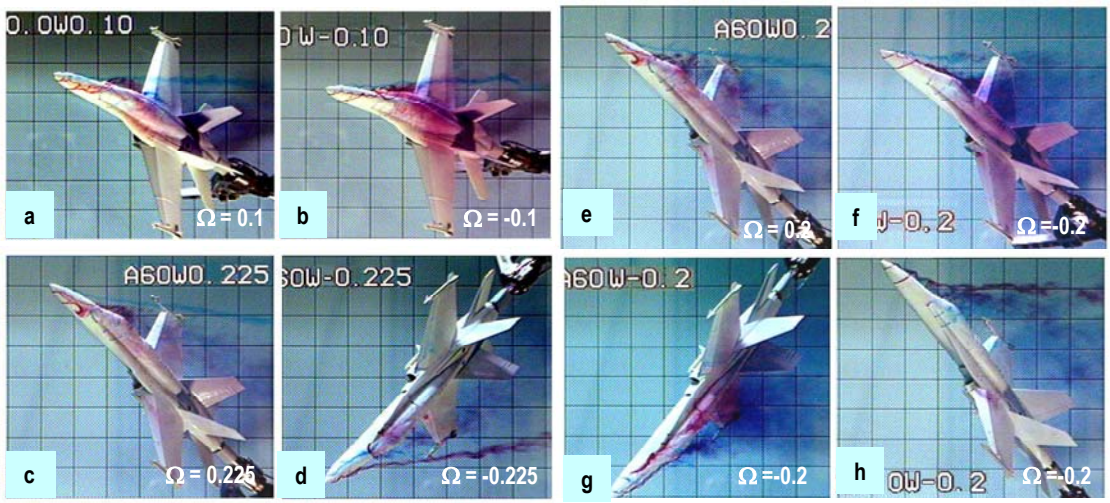

Fig. 12 Vortex flow field on coning model at $\alpha = 60$ deg

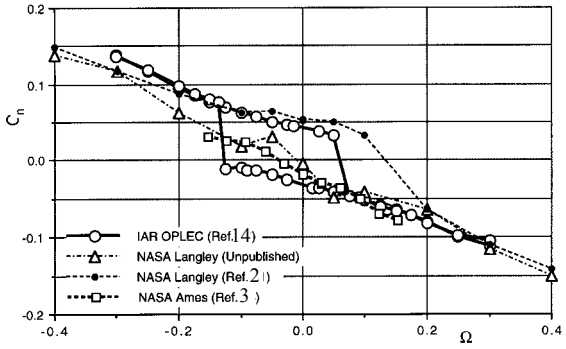

Fig. 13 Interfacility correlation of F/A-18 yawing moment at $\alpha = 60°$

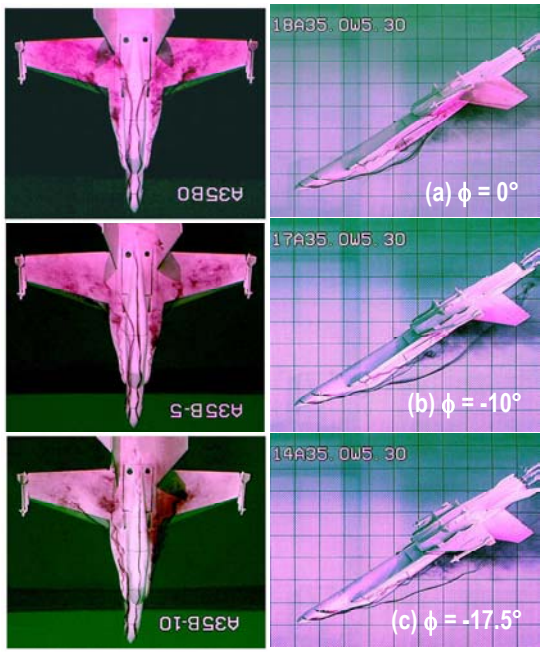

Fig.14 Forebody/LEX vortex interactions at $\sigma = 35°$ and three bank angles

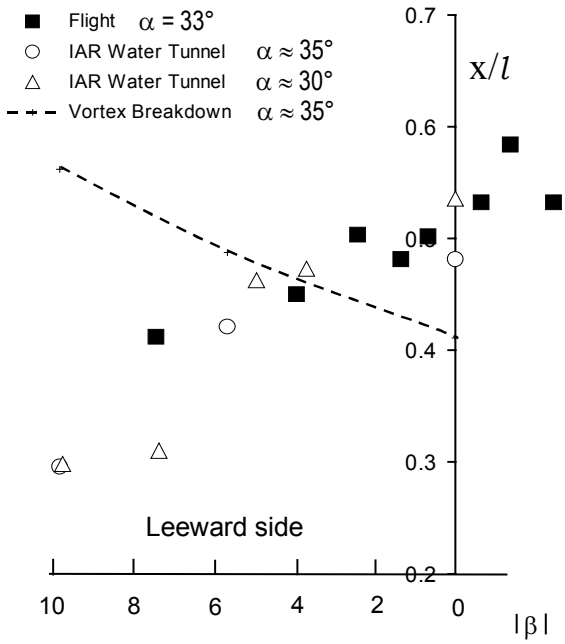

Fig. 15 Comparison of vortex interaction locations at $\beta \neq 0$ and $30° \leq \alpha \leq 35°$

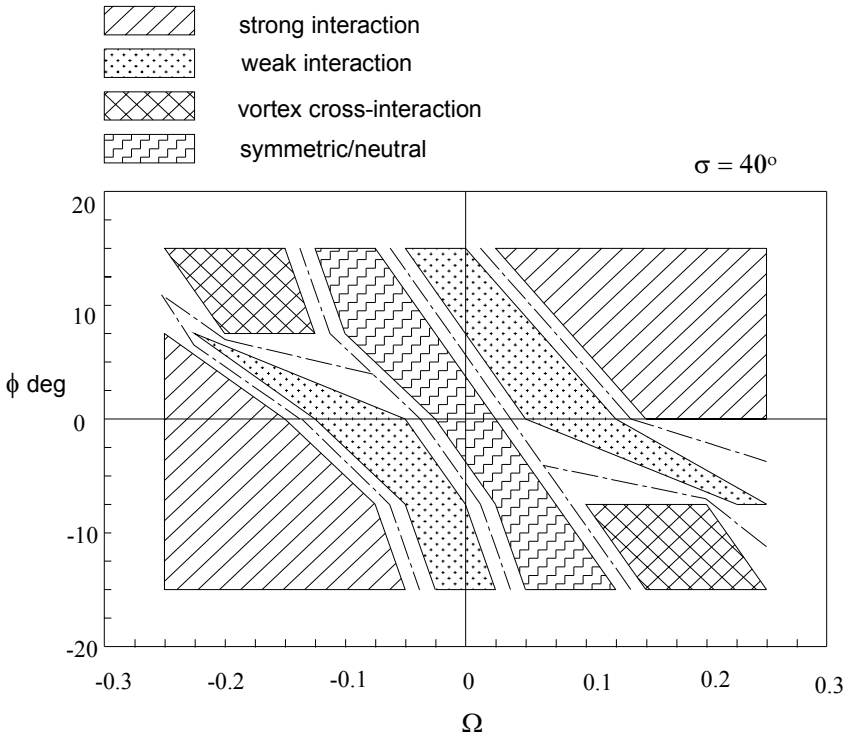

Fig. 16 Map of forebody/LEX vortex interaction conditions for $\sigma = 40$ deg, $\phi \neq 0$

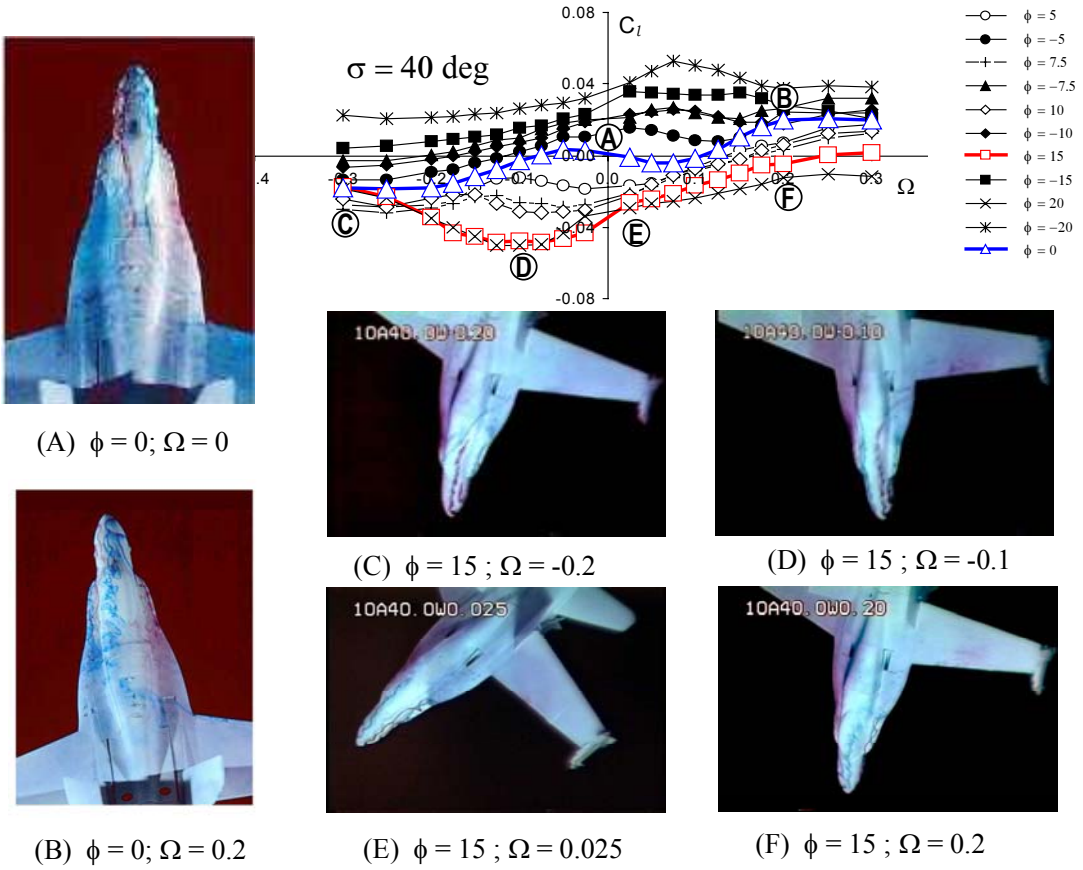

(A) $\phi = 0; \Omega = 0$

(B) $\phi = 0; \Omega = 0.2$

(C) $\phi = 15; \Omega = -0.2$

(D) $\phi = 15; \Omega = -0.1$

(E) $\phi = 15; \Omega = 0.025$

(F) $\phi = 15; \Omega = 0.2$

Fig. 17 Sideslip effect on forebody/LEX vortex interactions at various coning rates